REVIEW ARTICLE

A review of ultrasound common carotid artery image and video segmentation techniques

Christos P. Loizou

Abstract The determination of the wall thickness [intima–media thickness (IMT)], the delineation of the atherosclerotic carotid plaque, the measurement of the diameter in the common carotid artery (CCA), as well as the grading of its stenosis are important for the evaluation of the atherosclerosis disease. All these measurements are also considered to be significant markers for the clinical evaluation of the risk of stroke. A number of CCA segmentation techniques have been proposed in the last few years either for the segmentation of the intima–media complex (IMC), the lumen of the CCA, or for the atherosclerotic carotid plaque from ultrasound images or videos of the CCA. The present review study proposes and discusses the methods and systems introduced so far in the literature for performing automated or semi-automated segmentation in ultrasound images or videos of the CCA. These are based on edge detection, active contours, level sets, dynamic programming, local statistics, Hough transform, statistical modeling, neural networks, and an integration of the above methods. Furthermore, the performance of these systems is evaluated and discussed based on various evaluation metrics. We finally propose the best performing method that can be used for the segmentation of the IMC and the atherosclerotic carotid plaque in ultrasound images and videos. We end the present review study with a discussion of the different image and video CCA segmentation techniques, future perspectives, and further extension of these techniques to ultrasound video segmentation and wall tracking of the CCA. Future work on the segmentation of the CCA will be focused on the development of integrated segmentation systems for the complete segmentation of the CCA as well as the segmentation and motion analysis of the plaque and or the IMC from ultrasound video sequences of the CCA. These systems will improve the evaluation, follow up, and treatment of patients affected by advanced atherosclerosis disease conditions.

1 Introduction

Accurate, reliable, efficient, and precise measurements of the geometry of the common carotid artery (CCA) are important for assessing and managing the progress of carotid atherosclerosis as well as assessing the risk of stroke [27]. The intima–media thickness (IMT) of the CCA (see also Fig. 1) is the most common indicator of the development of cardiovascular disease (CVD) [84]. An increase of the IMT has been correlated with the incident of stroke events [3, 27, 84]. It has also been documented that the risk of stroke increases with the severity of carotid stenosis and is reduced after carotid endarterectomy [3]. The degree of internal carotid stenosis is the only well-established measurement that is used to assess the risk of stroke [22], and it is therefore used as a validated measure to decide whether carotid endarterectomy is indicated or not [38, 71]. It was reported that in stroke, high-risk patients with asymptomatic internal carotid artery stenosis >60–70 % carotid endarterectomy reduced the risk of stroke from 2 to 1 % per year [3, 22]. Thus, if patient subgroups with sufficiently higher than average risk, despite optimal medical

C. P. Loizou (✉)
Department of Computer Science, School of Sciences
and Engineering, Intercollege, 92 Ayias Phylaxeos Str.,
P. O. Box 51604, 3507 Limassol, Cyprus
e-mail: loizou.c@lim.intercollege.ac.cy;
panloicy@logosnet.cy.net
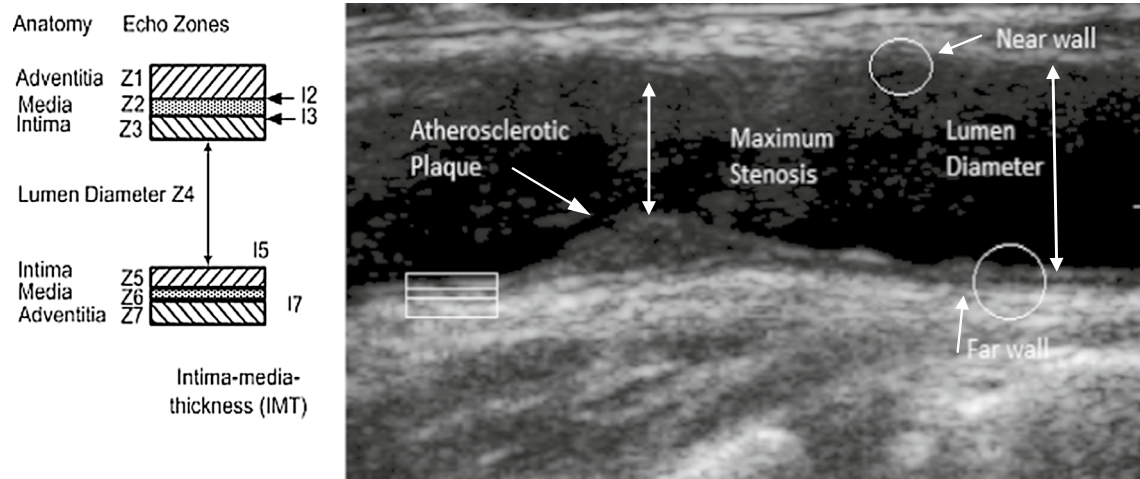
Fig. 1 Ultrasound image of the CCA and illustration of the intima–media complex (IMC) and the atherosclerotic carotid plaque at the far wall of the CCA, the lumen diameter, and the maximum carotid stenosis. The IMC consists of the intima band (Z5), the media band (Z6), and the far wall adventitia band (Z7). The IMT is defined as the distance between the blood–intima interface line and the media–adventitia interface line. See also [45]

intervention, could be reliably identified, then carotid surgery could be performed in those that are likely to benefit [3, 22, 71]. It has also been shown that IMT and plaque formation is a risk factor for stroke [72, 101], coronary artery disease [34], and myocardial infarction [8]. Carotid endarterectomy remains the gold standard, whereas carotid stenting retains its role in symptomatic patients at high risk of stroke [38]. Stenosis in the CCA is generated through the build-up of atherosclerotic carotid plaque formation (see also Fig. 1), which is due to progressive intimal accumulation of lipid, protein, and cholesterol esters in the blood vessel wall [113], which reduces blood flow significantly. Thus, monitoring the wall and plaque changes as well as the characteristics of the arterial wall in the CCA [52] and its elasticity [58] may have significant clinical relevance for the assessment of future cardiovascular events. It may also provide useful information for the assessment and management of the atherosclerotic disease.

The measurements and follow up of the IMT, the atherosclerotic carotid plaque, the CCA diameter, as well as grading of the artery stenosis, are imperative and are routinely assessed with high-resolution ultrasound imaging and video of the CCA [71]. Usually, delineations of the CCA are performed manually by medical experts [3, 22, 71, 84], but it was shown that these are subject to errors and have large variability between different experts, different equipment, and different datasets [30, 31, 45, 48–50, 52, 56, 58, 60, 65, 66]. Therefore, automated methods for the accurate and reliable delineation and measurement of the IMT [45, 48, 50, 52, 58, 65, 66], the atherosclerotic carotid plaque [30, 49, 60], and the CCA diameter [56] from ultrasound images or videos are required.

There is today an increasingly growing interest for the development of automated computer-based software systems for the segmentation of the CCA from ultrasound images and videos that can be integrated in the real clinical praxis. There are a number of methods proposed in the last 12 years either for the segmentation of the intima–media complex (IMC), the atherosclerotic carotid plaque, or the CCA diameter from ultrasound images and/or videos of the CCA, which are presented in Tables 1, 2, 3, 4. We also present an integrated system [56], for the complete segmentation of ultrasound images of the CCA. The system incorporates all above techniques such as that it allows the complete ultrasound image segmentation of the CCA. More specifically, the method proposed in [56] allows the segmentation of the IMC, the extraction of the atherosclerotic plaque, the delineation of the CCA diameter, and the grading of its stenosis. Nowadays, there are a few known commercial software-imaging systems supporting IMC segmentation available from different research groups [10, 103], which are based on snakes [9, 10, 15, 16, 39, 103], zip-lock snakes [102], gradient vector flow [107], dynamic programming (DP) segmentation [103], [45], neural networks [62], as well as integrated approaches [66, 68]. Recently, two different commercial software systems for ultrasound image [59], and video [57] analysis of the CCA, have been developed, can be downloaded, and used in the clinical praxis.

The bifurcation and the internal carotid artery are at more risk in atherosclerosis, due to stronger hemodynamic stresses in the bifurcation and branching zones [22, 38, 71], but it is difficult to visualize the double-line pattern in these locations. Therefore, IMT measurements in

Table 1 An overview of IMC segmentation techniques in 2D and 3D ultrasound imaging of the CCA

Investigator	Segmentation method	Year	Input	AIC	UI	MC	IMT$_{mean}$ ± std [mm]	User variability [mm]	Performance metrics	Processing time/frame [s]	IMT error × 10^{-3} [mm]	N
Destrempes et al. [18]	Nakagami Distributions	2009	USC	Yes	Yes	Yes	0.81 ± 0.13	–	MAD, HD	24	21 ± 13/1.6 ± 7	7,283
Molinari et al. [67]	Multi-resolution edge snapper	2012	USC	Yes	No	No	0.91 ± 0.44	0.83 ± 0.39	MAD	15	78 ± 112	365
Delsanto et al. [17]	Fuzzy C means and snakes	2007	USC	Yes	Yes	Yes	0.71 ± 0.16	–	MAD	–	63 ± 49.1	200
Faita et al. [23]	First-order edge operator	2008	USC	No	Yes	No	0.56 ± 0.14	0.559 ± 0.178/ 0.68 ± 0.184	MAD	–	1 ± 35	150
Loizou et al. [48]	Snakes	2007	USC	Yes	Yes	Yes	0.68 ± 0.12	0.0	MAD, HD, CV = 12.5 %, BA, Histograms	30	50 ± 25	100
Loizou et al. [50]	Snakes	2009	USC	Yes	Yes	Yes	0.67 ± 0.12	0.0	MAD, HD, CV = 12.6 %, BA, Histograms	27	8 ± 20	100
Santhiyakumari et al. [88]	Active contours	2011	USC	Yes	Yes	No	0.46 ± 0.03	0.55 ± 0.019	CV = 19 %, BA	–	90	100
Petroudi et al. [73]	Active contours and LS	2012	USC	Yes	Yes	No	0.61 ± 0.15	–	MAD, CV = 15 %	21	80 ± 70	100
Wendelhag et al. [103]	DP	1997	USC	No	Yes	Yes	0.92 ± 0.25	–	MAD, CV = 2 %	–	30 ± 32	69
Lara et al. [62]	Neural Networks	2013	USC	Yes	No	No	0.61 ± 0.19	0.614 ± 0.192	MAD, PLD, CLD, BA	–	38 ± 25	60
Liang et al. [45]	DP	2000	USC	No	Yes	Yes	0.93 ± 0.25	0.9342 ± 0.253	MAD	42	42 ± 20	50
Stein et al. [92]	Gradient based	2005	USC	Yes	Yes	Yes	0.67 ± 0.12	0.674 ± 0.127	MAD	–	12 ± 6	50
Xu et al. [108]	Hough and dual snake	2012	USC	No	Yes	No	0.65 ± 0.16	0.653 ± 0.162	MAD	0.465	20 ± 30	50
Ilea et al. [35]	Model based	2009	USC	Yes	No	No	–	–	MAD	8	79	49
Freire et al. [25]	Gradient based	2009	USC	No	Yes	No	0.53 ± 0.06	0.563 ± 0.06	BA, CV = 6.34 %	2.52 ± 0.38	5	43
Rossi et al. [83]	Anisotropic barycenter	2010	USC	Yes	No	No	–	–	BA	1.5	50	36
Cheng et al. [10]	Snakes	2002	USC	Yes	Yes	Yes	0.65 ± 0.16	–	MSE	–	92 ± 31.5	32
Gutierrez et al. [30]	Active contour and Balloon	2002	USC	No	Yes	Yes	0.72 ± 0.14	0.729 ± 0.146	CV = 19 %	31	–	30
Mojsilovic et al. [64]	Texture based	1997	IVUS	–	Yes	No	0.68	–	MAD	–	–	29
Selzer et al. [90]	Edge-tracking	2001	USC	No	Yes	Yes	0.78 ± 0.17	0.77 ± 0.16	MAD, CV = 4.03 %	15	–	24
Loizou et al. [56]	Snakes	2013	USC	Yes	Yes	Yes	0.93 ± 0.25	–	MAD, HD, BA	28	65 + 32	20
Golemati et al. [28]	Hough transform	2007	USC	No	–	–	0.61 ± 0.05	–	CV = 7 %	–	–	10
Mao et al. [61]	Discrete dynamic contour	2000	USC	No	Yes	No	–	–	–	–	–	7
Bastida-Jumila et al. [6]	Active contours	2013	USC	Yes	No	No	–	–	MAD	–	24.8	–
Xiao et al. [106]	Inhomogeneity correction	2002	USC	No	No	No	–	–	–	–	–	–
3D Studies												
Yang et al. [110]	Active shape model	2013	USC	Yes	No	No	0.75 ± 0.46	–	MAD, DSC	258 ± 30	0.26 ± 0.18	68

DP dynamic programming, *LS* level sets, *USC* ultrasound carotid images, *USC* ultrasound muscular arteries, *IVUS* intra-vascular ultrasound, *AIC* automatic initial contour, *UI* user interaction, *MC* manual corrections possible, *IMT$_{mean}$ ± std* Mean IMT ± standard deviation in mm, *MAD* Mean absolute difference in mm, *BA* Bland–Altman plots, *CV* Coefficient of variation, *DSC* Dice similarity, *N* Number of subjects investigated, *PLD* Polyline distance, *CLD* center line distance, *HD* Hausdorff distance, *MSE* Mean square error

the CCA are preferred in the development of segmentation algorithms and in clinical practice [31]. It has been shown that increased IMT reflects early stages of atherosclerosis and CVD risk, especially in older adults without a history of CVD [72]. Higher blood pressure and changes in shear stress are the potential causes of intimal thickening, which may cause a local delay in lumen transportation of potentially atherogenic particles that favors the accumulation of substances in the arterial wall and consequent plaque formation [101]. It is also found that type 1 diabetes is a significant risk factor for increased CCA IMT in children [37]. The measurements of the IMT in the prediction of the degree of atherosclerosis and the risk of stroke have been demonstrated by different studies [31, 101], [8–10, 15, 16, 30, 31, 34, 45, 48–50, 52, 56, 58, 60, 65, 66, 103, 113], where it was confirmed that the increase of the IMT value above 0.9–1.0 mm is indicative of a significant increase for the risk of stroke.

In Sect. 2, we present the clinical significance and challenges of the CCA segmentation measurements. Section 3 presents evaluation metrics for the segmentation methods, while Sect. 4 presents different segmentation methods proposed in the literature. In Sect. 5, we discuss and compare the different segmentation methods. Finally, Sect. 6 concludes and outlines future challenges and trends in CCA ultrasound image and video segmentation.

2 Clinical significance and challenges of the CCA segmentation

2.1 Clinical significance

A B-mode ultrasound image presented in Fig. 1 shows the IMC at the far wall of the CCA (echo zones Z5–Z6), as a pair of parallel bands, an echodense, and an echolucent band. Band Z5 and the leading edge of band Z7 (adventitia) are denoted as I5 and I7 and define the IMT of the far wall. With this understanding, the determination of the IMT at the far wall of the CCA becomes equivalent to accurately detecting the leading echo boundaries I5 and I7. The lumen–intima (I5) and media–adventitia (I7) intensity interfaces of the far wall of the CCA are preferred for IMT measurements [8, 45, 103]. It has been shown that the definition of the IMT as shown in Fig. 1 corresponds to the actual histological IMT [39, 43, 45]. Figure 1 also shows an atherosclerotic carotid plaque at the far wall of the CCA, the position of maximum lumen stenosis, as well as the lumen diameter, which is usually measured in an area where no atherosclerotic carotid plaques are present [22, 38, 71].

In practice, however, detecting the boundaries of the IMC and the atherosclerotic carotid plaque is often complicated by the presence of ultrasound imaging artefacts, such as speckle [46], making IMT [48], plaque [49], and CCA stenosis [56] measurements difficult to be accomplished. Furthermore, the observation of the IMC and plaque borders becomes more difficult as the age of patients increases, due to the presence of acoustic holes (echo-dropouts) in the adventitia layer [43, 104]. The intimal band may appear as a thin low-contrast structure, and therefore, it is difficult to reliably draw boundaries because smoothing can move the structure edges or make them disappear [64]. Traditionally, the IMT and the atherosclerotic carotid plaque are measured by manual delineation of the intima, the adventitia layer at the far wall, and the near wall of the CCA [45, 64, 103, 104]. Manual tracings of the lumen diameter (see Fig. 1, band Z4) and the IMT (see Fig. 1, bands I5 and I7) require substantial experience; it is time-consuming and varies according to the training, experience, and the subjective judgment of the experts [71, 30, 45, 48–50, 56, 60, 65, 66]. The manual measurements suffer therefore from considerable inter- and intra-observer variability [45, 103, 104]. It was furthermore reported in [75–77, 97] that the accuracy of manual tracings is not reproducible and that manual tracings suffer from high intra- and inter-user variability. More specifically, in [76], 26 CCA ultrasound images were delineated by 5 clinical experts and significant different inter-reader differences were found, which may affect correct evaluation of the CVD risk. In contrast, it was shown in [77] that the application of automated computer-based analysis of the CCA may reduce variability. In [75, 97], it was shown that there are inter- and intra-reader bias when manually tracing the borders of the artery.

The importance of the IMC, the CCA segmentation, and stenosis measurements has been indicated in 1986 by Pignoli et al. [74], who concluded that B-mode imaging is a very useful approach for the measurement and visualization of the IMC and plaque at the far wall of the CCA. Increased IMT was demonstrated to have a strong correlation with the presence of atherosclerosis elsewhere in the body and may thus be used as a descriptive index of individual atherosclerosis [43]. As vascular disease develops, local changes occur in arterial structure, which thicken the innermost vessel layers (IMC). As disease progresses, the IMT initially increases diffusely along the artery and then becomes more focal, forming discrete lesions or plaques, which gradually grow and obstruct blood flow. Furthermore, these plaques can become unstable and rupture with debris transported distally by blood to obstruct more distal vessels. This is particular so if plaques develop internal pools of lipid covered only by a thin fibrous cap [8, 43]. In [5], it was also documented that carotid IMT and plaque are important in vascular disease risk prediction.

2.2 Challenges in CCA segmentation

The problems that are associated with the computer-assisted border tracing segmentation procedures (also presented in Tables 1, 2, 3, 4) are the following: (1) They do not take into consideration the speckle noise or the image intensity normalization in the ultrasound images [64], or videos [54, 55, 58]. (2) They are sensitive to the initial snake contour [10], or initial seed points, which need to be placed manually [111]. If the initial contour is placed far away from the boundary of interest, then the snake will not be attracted [10]. (3) Some weighting factors that should be tuned due to the varied characteristics of the ultrasound instrumentation must be entered manually or empirically [64, 103, 106, 111]. Some other weights may be adjusted by a training procedure, which might be long and requires expert tracing [45, 61]. (4) The snake is implemented as a close contour [15, 105, 111] that might not be very suitable for the IMC segmentation. (5) They require manual correction after automatic tracing [10, 61, 64, 103]. (6) In a number of cases, there were no ground truth segmentation delineations from experts to compare with the computer-assisted methods [10, 64]. (7) Different measurement procedures were used between the manual and the automated snakes segmentation methodologies [10, 45, 61, 103]. (8) Different criteria were used for assessing the performance of the segmentation algorithms [10, 111]. (9) They are evaluated on a limited number of images or videos, where the intra- and inter-observer variability could not be assessed [61, 106]. In order to take into considerations some of the above challenges, ultrasound image and video normalization followed by speckle reduction filtering [46, 48, 49, 58] were proposed. These techniques are described in Sect. 4.1.

3 Evaluation metrics for the segmentation methods

In order to evaluate their segmentation methods, different authors compare them with the manual delineation results, made by specialists (usually one or two), which are considered to be the ground truth. The following performance evaluation metrics may be used:

The mean absolute difference (MAD) can be estimated using the manual and automated measurements as follows [45, 52, 58, 66]:

$$\text{MAD} = \frac{1}{N} \left| \sum_{n=1}^{N} (\text{Manual}_n - \text{Automated}_n) \right| \quad (1)$$

where N is the number of points included in the two boundaries (manual and automated) and n is the index indicating the number of points defined on each boundary. In the case

where the two boundaries do not have the same number of points, then one of them can be interpolated. This metric is particularly suitable when the borders of the artery wall are horizontal, and they do not include curved segments, in which case, the MAD is overestimated. The equation in (1) can be used also to estimate the error between the two measurements as follows:

$$\text{Err} = \frac{1}{P} \left| \sum_{n=1}^{P} (\text{Manual}_n - \text{Automated}_n) \right| \quad (2)$$

where P is the total number of processed images delineated, and Manual_n and Automated_n are the manual and automated measurements for each image.

The parameters IMT_{mean}, IMT_{min}, IMT_{max}, and IMT_{median}, as well as the intra- and inter-observer error [45, 103], se $= \sigma_{IMT}/\sqrt{2}$, with σ_{IMT}, the standard deviation of the automated measurements, were used to evaluate the segmentation method. The coefficient of variation, CV %, which describes the difference as a percentage of the pooled mean value (IMT_{pooled_mean}) [45, 103] can be used as follows:

$$\text{CV\%} = \frac{\text{se}}{\text{IMT}_{pooled\_mean}} 100 \quad (3)$$

The Wilcoxon matched pairs rank sum test [20], which calculates the difference between the sum of the ranks of two independent samples, is used in order to identify whether for each set of measurements, a significant difference (S) or not (NS) exists between the manual and the automated, at $p < 0.05$. Additionally, the correlation coefficient, ρ, between the manual and the automated measurements is investigated, which reflects the extent of a linear relationship between two data sets [9].

Furthermore, the Hausdorff distance (HD) [9] between the two curves (m: manual and a: automated) could be calculated. It reflects the maximum mismatch between the manual and the snakes segmented areas, where small values for the HD are favorable $\text{HD} = \max\{d_m, d_a\}$. The major limitation of HD is that only distances between points are measured. Therefore, this measure is significant when the two boundaries have almost the same number of points. In order to assess the intra-observer variability between different experts, the manual measurements are repeated after a period of time.

In some cases, the polyline distance (PLD) [94] may also be computed, which has been shown [65] to be a more reliable and robust indicator of the distance between two given boundaries [85], which truly represents the distances between boundary shapes along the artery. The basic idea is to measure the distance of each vertex of a boundary to the segments of the other boundary [65]. Similar metrics such

Table 2 An overview of IMC segmentation techniques in 2D ultrasound video of the CCA

Investigator	Segmentation method	Year	Input	AIC	UI	MC	IMT$_{mean}$ ± std [mm]	Performance metrics	Processing time/ frame [s]	IMT error [mm]	N
Zahnd et al. [112]	DP	2013	USV	Yes	No	No	0.74 ± 0.09	MAD	–	0.029 ± 0.027	82
Ilea et al. [36]	Model based	2013	USV	Yes	Yes	No	0.60 ± 0.10	MAD	80 (8 in 1st frame) and 72 for 28 frames	0.007 ± 0.176	40
Loizou et al. [54]	Snakes	2013	USV	Yes	Yes	Yes	0.72 ± 0.22	MAD, CV = 13 %, BA	20	0.008 ± 0.02	10
Cheng et al. [11]	DP	2010	USV	Yes	No	No	0.56	MSE	–	0.0668, 0.0583	3

DP Dynamic Programming, *USV* Ultrasound carotid videos, *AIC* Automatic initial contour, *UI* user interaction, *MC* Manual correction possible, *IMT$_{mean}$ ± std* Mean IMT ± standard deviation in mm, *N* Number of subjects investigated, *MAD* Mean absolute distance, *CV* Coefficient of Variation, *BA* Bland–Altman plots

Table 3 An overview of plaque segmentation techniques in 2D and 3D ultrasound imaging of the CCA

Investigator	Segmentation method	Year	AIC	UI	MC	TPF (%)	Performance metrics	Processing time/frame [secs]	N
Loizou et al. [49]	Snakes	2007	Yes	Yes	Yes	(82.70 ± 2.1)[a]	KI = 80.66 %, O = 66.6 %, Sp = 0.937, P = 0.926	17	80
Delsanto et al. [17]	K-means fuzzy gradient	2007	No	No	–	–	–	20	56
Rocha et al. [79]	Dynamic Programming	2010	Yes	No	No	95	MAD, BA		47
Golemati et al. [28]	Hough transform	2007	No	–	–	(97.5 ± 1.0)	–	0.04	4
Hamou et al. [32]	Canny edge detection	2004	No	–	–	–	–	–	2
Abdel-Dayen et al. [1]	Morphological based	2004	No	–	–	–	–	–	2
Abolmaesumi et al. [2]	Kalman filtering	2000	No	–	–	–	–	–	1
Guerrero et al. [29]	Star Kalman	2007	No	–	–	–	–	–	–
Slabaugh et al. [91]	Region Active Contour	2009	No	–	–	–	–	–	–
3D Studies									
Zahalka et al. [111]	Geometrically deformable model	2001	Yes	Yes	Yes	TPF = 95	–	25	69
Cheng et al. [12]	Level set	2012	Yes	No	No	96.7 ± 1.7	–	–	36
Ukwatta et al. [100]	Level sets	2013	No	–	–	94.4 ± 2.2	CV = 5.1 %, ISD = 0.2 ± 0.1 mm	103.2	21
Gill et al. [26]	Balloon	2000	No	No	No	–	–	–	2

USC ultrasound carotid images, *IVUS* intra-vascular ultrasound, *AIC* automatic initial contour, *UI* user interaction, *MC* manual corrections possible, *TPF; TNF* true-positive and true-negative fractions, *FPF, FNF* false-positive and false-negative fractions, *KI* Williams index, *O* Overlap, *Sp* specificity, *P* precision, *MAD* mean absolute difference, *BA* Bland–Altman plots, *CV* coefficient of variation, *ISD* inter-slice distance, *N* number of subjects investigated

[a] In [49] TNF = (80.89 ± 1.9) %, FPF = (5.86 ± 1.8) %, FNF = (15.59 ± 1.1) %

as the PLD were also employed in [62], such as the mean absolute distance (MAD) and the center line distance (CLD).

Bland–Altman plots [7], with 95 % confidence intervals, were also used to further evaluate the agreement between the manual and the automated segmentation measurements. Regression analysis [20] was also used to demonstrate the relationship between the manual and the automated segmentation measurements. Furthermore, box plots for the manual and the automated measurements can be plotted, as well as the Pearson's correlation coefficient, ρ, between these measurements which investigate their agreement.

In some cases, histograms of the measurements are also plotted, as well as error histograms [17], in order to fully characterize the IMT estimation errors. In [10], the mean squared error was used to evaluate the segmentation method. This performance metric does, however, allow for determining underestimations or overestimations of the IMT and therefore does not represent an optimal choice. A number of other evaluation metrics for image segmentation can also be found in [99, 114].

In some other studies, where the segmentation of the atherosclerotic carotid plaque was proposed (see also

Table 4 An overview of plaque segmentation techniques in 2D ultrasound video of the CCA

Investigator	Segmentation method	Year	Input	AIC	UI	MC	TPF	Performance metrics	Processing time/frame [s]	N
Loizou et al. [58]	Snakes	2013	USV	Yes	Yes	Yes	(86.1 ± 8.0) %	TNF = (84.3 ± 7.5) %, KI = 85.3 %, O = 75.4 %	9	43
Destrempes et al. [19]	Bayesian model	2011	USV	No	No	No	(83.7 ± 8.3) %	TNF = (83.7 ± 8.3) %, KI = 84.8 %, O = 74.6 %, HD = (1.24 ± 0.4) mm, MPD = (0.24 ± 0.08) mm	30	33

USV ultrasound videos, *AIC* automatic initial contour, *UI* user interaction, *MC* manual corrections possible, *TPF, TNF* true-positive and true-negative fraction, *KI* Williams index, *O* overlap, *HD* Hausdorff distance, *MPD* mean point distance, *N* number of subjects investigated

Manual Segmentations   Snakes Based Segmentations
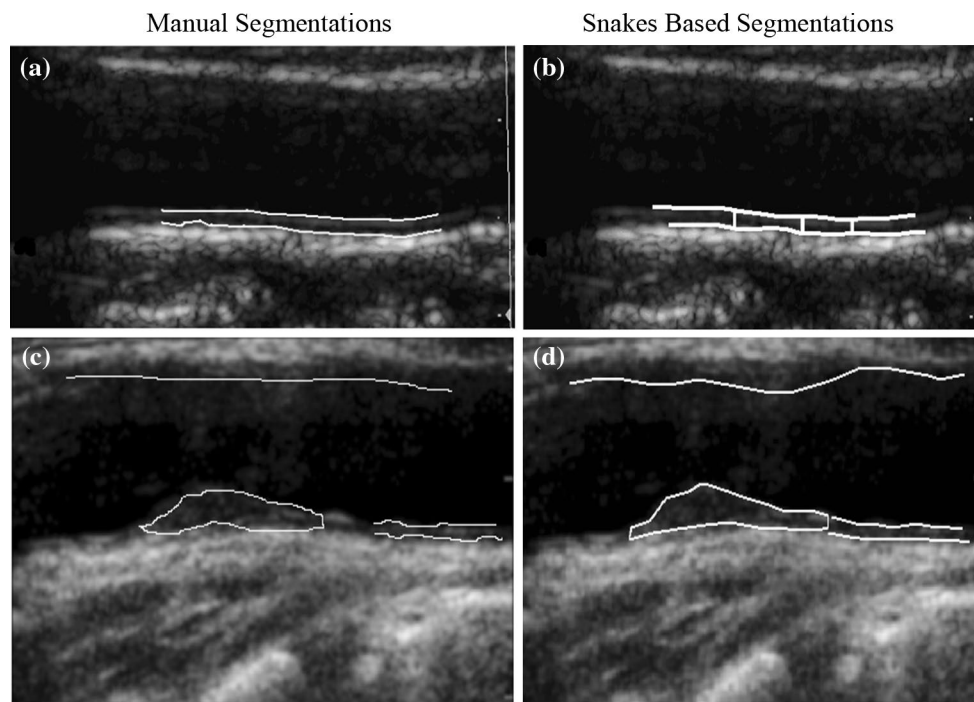
Fig. 2 **a** Normalized despeckled ultrasound image of the CCA from an asymptomatic subject at the age of 54, with manual delineation of the IMC from the expert (IMT_{mean} = 0.67 mm), **b** automated segmentation of the IMC by snakes [48, 50] on the normalized despeckled ultrasound image (despeckled with the DsFlsmv filter) of the CCA of **a** (IMT_{mean} = 0.68 mm, IMT_{max} = 0.91 mm, IMT_{min} = 0.43 mm, IMT_{median} = 0.66 mm), **c** Normalized despeckled ultrasound image of the CCA from an symptomatic subject at the age of 63, with an atherosclerotic carotid plaque at the far wall of the artery IMC (IMT_{mean} = 0.91 mm), and the near wall, and manual delineations from the expert, **d** Complete segmentation [56] of the CCA on the normalized despeckled ultrasound image of **c** (IMT_{mean} = 0.936 mm, IMT_{max} = 1.01 mm, IMT_{min} = 0.77 mm, IMT_{median} = 0.966 mm, lumen diameter = 6.84 mm, lumen diameter at maximum point stenosis = 5.44 mm, plaque major axis (width) = 13.58 mm, and plaque minor axis (height) = 1.97 mm)

Table 3), different other performance metrics were applied. These include the receiver operating characteristic (ROC) analysis [63], which assesses the specificity and sensitivity of the segmentation methods by the true-positive fraction (TPF), false-positive fraction (FPF), true-negative fraction (TNF), and false-negative fraction (FNF) [49, 58, 63]. Ratios of overlapping areas can also be assessed by applying the similarity kappa index KI [24] and the overlap index [81]. Furthermore, the specificity Sp = 1 − FPF and the precision P can also be calculated to describe the ROC characteristics of the segmentation methods, as well as the inter-slice distance [100]. Finally, in [13], statistical metrics to evaluate the difference of local vessel wall thickness of the CCA in 3D ultrasound images between manual and

automated segmentations were proposed. The difference of the measurements produced maps with which the segmentation method can be evaluated.

4 Automated CCA segmentation techniques

There are a number of segmentation techniques that have been developed so far for the ultrasound image or the video segmentation of the IMC (see Tables 1, 2) and the atherosclerotic carotid plaque (see Tables 3, 4). These techniques can be grouped into edge- and gradient-based, DP, snake- and level set-based, Nakagami modeling, Hough transform, neural networks, and integration of the above techniques. The methods presented in Tables 1, 2, 3, 4 have been grouped based on the number of subjects (*N*) investigated. Before proceeding with the segmentation of the structure of interest, some authors proposed automated procedures using morphology features [65], the Hough transform [28], or parametrical template matching [82], for recognizing and creating a guidance zone around the IMC, or the atherosclerotic carotid plaque. The idea is that the area of interest can be cropped; thus, the size of the image to be segmented can be significantly smaller.

4.1 IMC image segmentation techniques

Pignoli et al. [74] were the first to introduce a computerized method for the IMC segmentation in ultrasound images of the CCA. They measured the IMT at the far wall of the CCA by considering the intensity profile of the far wall when moving from the center of the vessel to the wall borders. Four years later, Touboul et al. [96] proposed an IMT segmentation method based on edge detection, which was used and applied in several clinical and epidemiological studies [98]. A good agreement with the manual measurements was found with a correlation coefficient of 97 %.

In Fig. 2a, we present a normalized despeckled ultrasound image of the CCA from an asymptomatic subject aged 54, with the manual delineation of the IMC from the expert, while in Fig. 2b, we show the automated segmentation of the IMC by snakes at the far wall on the normalized despeckled ultrasound image of the CCA in Fig. 2 a. The automated segmentations were performed using the snakes-based segmentation system proposed in [48].

In the following, we describe the most performing techniques for the CCA IMC segmentation in 2D and 3D ultrasound imaging, which are also summarized in Table 1.

Destrempes et al. [18] introduced a semi-automated segmentation method to segment the IMC, by taking into consideration various dynamical properties of the tissue, such as the elasticity distribution (elastogram), which was modeled by a mixture of three Nakagami distributions. The method required manual intervention. Different assumptions were taken for the segmentation of the CCA in [18], which offers limited applicability to the method, particularly when calcified plaques are presented. Additionally, the authors did not take into consideration the speckle noise in the image. Mollinari et al. [67] used a multi-resolution edge snapper which was based on an additional external energy term (edge snapper, FOAM), which prevented premature collapses of the snake contour. Delsanto et al. [17] proposed a user-independent system combined approach for the IMC segmentation, based on local statistics and snakes. The CCA was automatically located by clustering the image into a bidimensional histogram and computing the mean and standard deviation values of the image pixels in a 10×10 neighborhood by considering the image column-wise and by identifying the lumen using a uni-modal histogram. Speckle noise caused problems for the proper IMC segmentation in about 10 % of the cases. The technique was also applied in curved vessels with non-horizontal appearance. In [23], a first-order absolute moment (FOAM) edge operator [65] was used as an additional term in the snake's energy for the segmentation of the IMC. The technique was robust to curved vessels. Full automation is precluded by the need for a manual selection of an ROI in the CCA image. Loizou et al. [48, 50] used snakes to segment the IMC [48], the intima, media, and the adventitia layers [50] of the CCA by incorporating additional terms in the snake energy functional. Furthermore, initial snake contour estimation, image normalization [47], and speckle noise reduction filtering [46] were employed. A limitation is the presence of acoustic shadowing, which hinders the visual and automatic analysis in ultrasound images [45, 50, 103].

In all studies performed by our group [46–50, 52, 54–59], the images and videos used were recorded at the Cyprus Institute of Neurology and Genetics, in Nicosia, from asymptomatic (at risk of atherosclerosis) or symptomatic subjects. The symptomatic subjects were at risk of atherosclerosis and have already developed clinical symptoms, such as a stroke or a transient ischemic attack, while the asymptomatic did not develop any clinical symptoms. Two different ultrasound scanners were utilized in this study to acquire the images of tag image file format (*.tif) and videos of audio–video interleave format (*.avi), respectively. The two scanners used were the ATL HDI-3000 and the ATL HDI-5000 (Advanced Technology Laboratories, Seattle, USA). Before proceeding with the segmentation, the images and/or videos [54, 55, 58] were intensity-normalized based on the method introduced in [21]. This improves image compatibility by reducing the variability introduced by different gain settings, different operators, different equipment, and facilitates ultrasound tissue

comparability [21, 95]. For the images, algebraic (linear) scaling is performed by linearly adjusting the image so that the median gray-level value of the blood was 0–5, and the median gray level of the adventitia (artery wall) was 180–190 [21]. Although the degree of interaction is still crucial in the segmentation process, to the best of our knowledge, no automated method exists for achieving image intensity normalization of the CCA. Further details can be found on image [5, 39, 41, 46–50, 56, 64, 74–77, 97, 104, 111] and video [54, 55, 58] normalization in publications made by our group.

Following image or video normalization, speckle reduction filtering in images and videos can be applied for reducing multiplicative noise. Despeckle filtering increases the visual perception evaluation and the accuracy of automated segmentation algorithms [20]. Several studies performed by our groups on ultrasound images [46, 47] and videos [5, 55, 58] for the despeckling of the CCA showed that the most appropriate despeckle filtering method for ultrasound images and videos of the CCA is the DsFlsmv filter (despeckle filter linear scaling mean variance), first introduced in [44]. The DsFlsmv filter can be applied to each image, while for the videos, the same filter is applied to each consecutive frame prior to the CCA segmentation. A complete description of the DsFlsmv filter for images can be found in [46, 47, 59], while for videos can be found in [46, 57]. An example of the application of the DsFlsmv filter is shown in Fig. 2, which was applied after image intensity normalization on the whole image. Before proceeding with the automated segmentation, vascular experts are delineating manually (using the mouse) the IMC [48, 50], the plaque [49], and the diameter [56] on ultrasound images [5, 39, 41, 46–50, 56, 64, 74–77, 97, 104, 111], or videos [54, 55, 58] of the CCA after image normalization and despeckle filtering. The manual delineations can be performed using a system implemented in MATLAB® by our group where the measurements are made between 1 and 2 cm proximal to the bifurcation of the CCA on the far wall [74]. Before running the image or video segmentation algorithm, IMC and plaque initialization procedures for positioning the initial snake contour in the image [49], or in the first video frame [54, 58], may be applied. The procedure will locate the approximate area of interest (IMC and plaque borders) where segmentation should be applied. An initialization method for the IMC was proposed in [48], while two different initialization methods for the atherosclerotic carotid plaque were introduced in [58]. A normalized despeckled image of a CCA video is shown in Fig. 3a. It is also assumed that the CCA is properly imaged in the video according to the standard clinical guidelines.

Active contours with ROI selection and speckle reduction filtering were applied in [88] and compared with a DP segmentation method [87], proposed by the same authors (see also Table 1). It was shown that the active contour [88]-based method performs better. In [73], active contours and level sets were combined to segment the IMC with initial contour estimation and speckle reduction filtering. The results were slightly better than the results reported in [48] and [50]. In [103], a DP method was presented, but it was operator dependent, required time to segment the IMC, while also speckle noise was not taken into consideration. Lara et al. [62] applied neural networks performing binary classification to estimate the IMC contours where also multilayer preceptors were employed. A multi-scale DP approach was proposed by Liang et al. [45], which was time-consuming with large differences between manual versus automated IMT measurements. The method proposed in [45] was later developed by Sundholm et al. [93], into a semi-automated CCA border detection software. In [92], a gradient-based semi-automated ultrasound border detection technique that facilitates clinical measurement of ultrasound carotid IMT was proposed where relatively small CV % was reported (CV % = 5.4 and 3.4 % for the manual and the automated methods). Furthermore, it was shown in [92] that the automated IMT measurements were faster, more reproducible, accurate, and independent of the operator skill. The method proposed in [92] did not perform on a real CCA wall segmentation, but rather was a computer system to aid and improve IMT estimation. Furthermore, no discussion was made about noise robustness. In [108], the Hough Transform and dual snakes were applied for the segmentation of the IMC. The method has robustness against ultrasound artefacts (although speckle reduction filtering was not applied) and gave better results than traditional snake model and DP-based methods. The segmentation fails when atherosclerotic plaques and small structures are presented primarily due to the presence of speckle noise. A model-based approach was proposed in [35], which relies on a suite of image processing algorithms. It embeds a statistical model to identify the two interfaces that form the IMT without any user intervention. The method was based on a spatially continuous vascular model and consists of several steps including data preprocessing, edge filtering, model selection, edge reconstruction, and data refinement. It was found to be robust in accurately estimating the IMT. Fraire et al. [25] introduced a gradient-based segmentation method for the IMC, which was applied on 43 ultrasound images of the CCA. The variation and the repeatability coefficients were better for the automated than the manual measurements. In [83], an automated algorithm to estimate CCA diameter and IMT in ultrasound images was proposed. The method also provides a visual scan quality feedback aimed to inform the sonographer about the adequacy of the insonation plane. In [10], snakes were used with initial snake contour estimation, which required user interaction, and the snake was attracted far away from the boundaries of interest in case

Manual Segmentations   Snakes based Segmentations
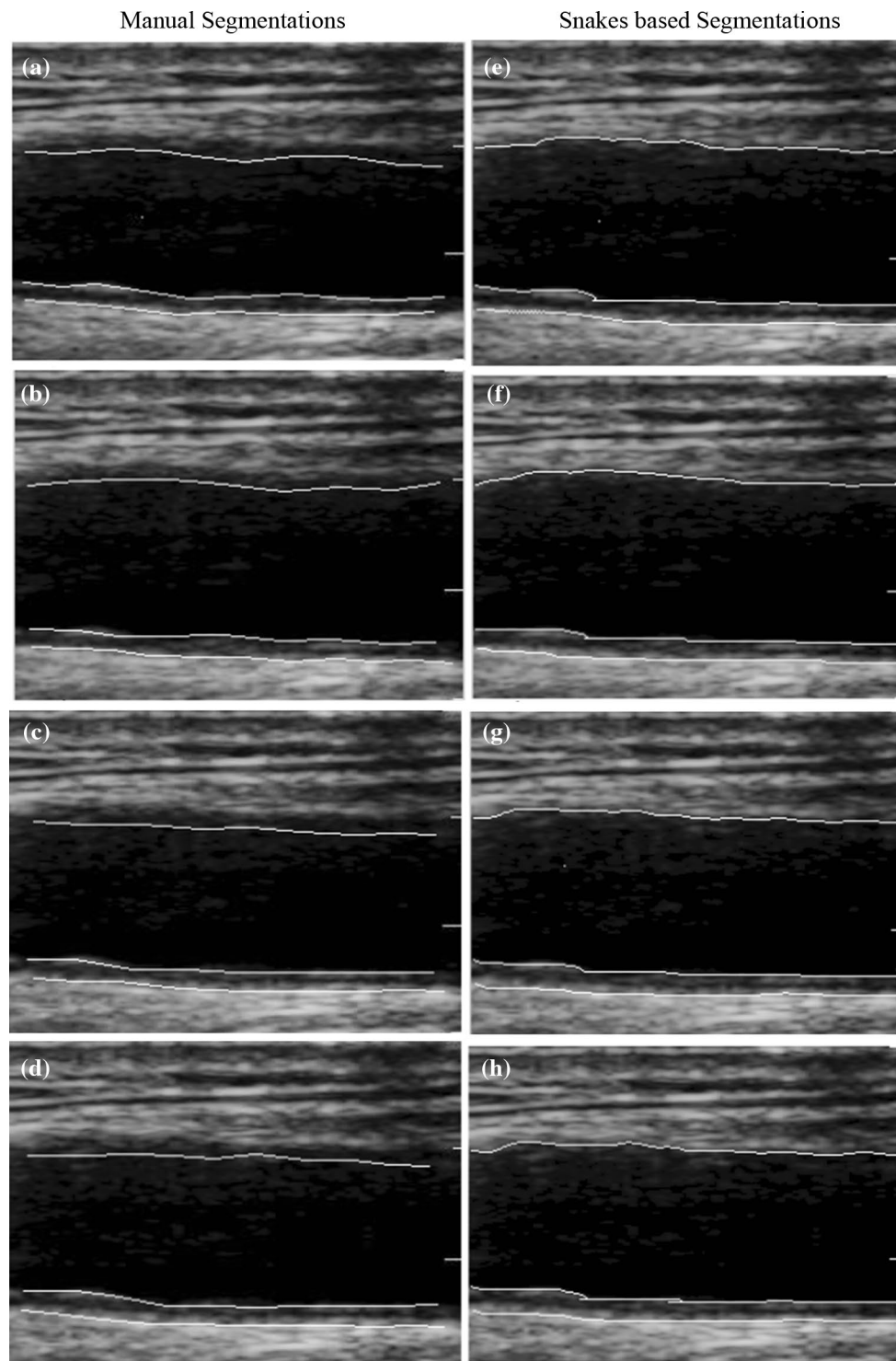
Fig. 3 Manual (*left column*) and automated (*right column*) video segmentation of the CCA for the IMT and carotid diameter [54], at the **a** 1st (IMT_{man} = 0.85 mm, $diameter_{man}$ = 6.69 mm, IMT = 0.99 mm, diameter = 6.9 mm), **b** 50th (IMT_{man} = 0.90 mm, $diameter_{man}$ = 7.31 mm, IMT = 0.93 mm, diameter = 7.51 mm), **c** 100th (IMT_{man} = 0.92 mm, $diameter_{man}$ = 6.98 mm, IMT = 0.95 mm, diameter = 7.21 mm), and **d** 150th (IMT_{man} = 0.90 mm, $diameter_{man}$ = 7.11 mm, IMT = 0.93 mm, diameter = 7.31 mm) video frames of the video

of curved segments and when speckle noise was present. In another study [30], an active contour and a Balloon model were used to segment the IMC where low agreement between manual and automated measurements was reported. Additionally, they reported a large manual versus automated segmentation CV % (14 vs 12.8 %). The authors reported problems with speckle noise, irregular boundaries, and curved segments where the snake was not well attracted. Mojsilovic et al. [64] extended Wendelhag's approach in [103], using DP with cost function optimization and applied histogram equalization for increasing the image contrast. Selzer et al. [90] performed a study for measuring automatically the IMT based on an edge-tracking procedure and reported a CV % of 4.03 and 3.46 % for the IMT measured at maximum and minimum diameter of the CCA, respectively. In [28], a method based on Hough transform was proposed, which required user interaction in order to produce the final segmentation boundary. Furthermore, the method took a long time to segment the IMC. An IMC segmentation approach with initial contour estimation based on a discrete dynamic contour was proposed in [61], which was derived from the entropy image using an initial circle matching procedure. In another study [6], a frequency implementation of active contours was proposed for the segmentation of the artery walls, while in [106], segmentation was achieved utilizing intensity inhomogeneity correction. Finally in [110], an active shape model was used in 3D CCA ultrasound images where large IMT differences with the manual tracings were reported due to weak image edges and speckle noise.

4.2 IMC video segmentation techniques

There are only a few studies proposed in the literature for the video segmentation of the IMC [11, 36, 54, 112], which are presented in Table 2. More specifically, in [112], the association between atherosclerosis risk factors and the cyclic variation of the IMT during the heart beat was investigated, by extracting the IMC from ultrasound video sequences using a DP method. The method proposed in [112] may provide a relevant diagnostic aid for atherosclerosis screening in clinical studies. In [36], a model-based CCA segmentation method was introduced, for the segmentation of the IMC, from ultrasound videos of the CCA. In [54], the IMC was segmented from ultrasound carotid videos using video despeckle filtering [55], and it was based on a snake segmentation method. Finally, in [11], a dual DP technique was applied for the video segmentation of the IMC for both far and near walls of the CCA.

In Fig. 3, we present manual (left column) and automated (right column) video segmentations of the CCA for the IMT and the carotid diameter, at the (a) 1st, (b) 50th, (c) 100th, and (d) 150th video frames of the video,

respectively. The automated IMC video segmentations were generated using the integrated segmentation system proposed in [54]. The video was acquired from a male asymptomatic subject aged 63 at risk of atherosclerosis.

4.3 Atherosclerotic carotid plaque image segmentation techniques

In Table 3, we present the methods developed so far for the segmentation of the atherosclerotic carotid plaque in CCA ultrasound imaging. Loizou et al. [49] applied an integrated snakes-based segmentation method, which incorporates automated initial contour estimation, image normalization, and despeckle filtering. In [17], a k-means gradient method to segment the carotid plaque based on a user-independent algorithm was proposed where it was shown that the segmentation error is lower than 1 pixel for both the lumen–intima interface and for the media–adventitia interface. In [79], the adventitia of the CCA was detected with an algorithm that searches for the best fit of a cubic spline to the adventitia contour. The lumen boundary is then estimated by another algorithm that uses the information of the adventitia location and combines DP in the presence of plaques, it has a strong computational load, and it is unable to capture deep concavities and sharp saliences. Another limitation is the difficulty in integrating global smoothing constraints, which could help improve the poor response at degraded parts of the lumen boundary. The method proposed in [79] was also later applied in [80] for the automated detection of the lumen in CCA B-mode images using a Gaussian smoothed filter and then a dynamic programming scheme, which extracts the dominant paths of local minima of the intensity and the dominant paths of local maxima of the gradient magnitude with the gradient pointing downwards. Similar results were reported in [79], but with a greater accuracy (99.5 %). The authors in [28] applied the Hough transform to automatically extract straight lines and circles from sequences of B-mode ultrasound images of longitudinal and transverse sections, respectively, of the CCA. Hamou et al. [32] proposed a method that was based on the Canny edge detector to detect the plaque regions, prior histogram equalization, in longitudinal 2D CCA ultrasound images. Abdel-Dayen et al. [1] used a morphological approach for the carotid contour extraction for longitudinal ultrasound images of the CCA, incorporating speckle reduction filtering, contour quantization, morphological contour detection, and a contour enhancement stage. Abolmaesumi et al. [2] introduced an algorithm based on the star algorithm improved by Kalman filtering, for extracting the CCA boundaries from transversal ultrasound images. Guerrero et al. [29] used a modified star Kalman approach to determine vessel contours and ellipse parameters using an extended Kalman filter with an elliptical model. Results indicate that mean errors between segmented contours and expert tracings are on the order of 1–2 % of the

maximum feature dimension and that the transverse cross-sectional vessel area was within 10 % of that determined by experts. Slabaugh [91] presented an ultrasound-specific segmentation approach that addresses both the spatial correlation of the data, as well as its intensity distribution by applying a region-based active contour.

In [111], an automated initial contour identification, followed by application of a geometrically deformable model, was proposed in 3D ultrasound CCA images. A fully automated segmentation method based on media–adventitia and lumen–intima boundary priors was proposed in [12] and also earlier in [40], for the segmentation of atherosclerotic carotid plaque in 3D CCA ultrasound images. The method combined image intensity with structure information in both initialization and a level set evolution process. Evaluation results indicated that the algorithm yielded total plaque volume differences of (-5.3 ± 12.7) mm^3 and (-8.5 ± 13.8) mm^3 and absolute true-positive volume (TPV) differences of (9.9 ± 9.5) mm^3 and (11.8 ± 11.1) mm^3 between the two experts. Moreover, high correlation coefficients in generating TPV (0.993 and 0.992) between algorithm results and both sets of manual results were obtained. Ukwatta et al. in [100] used level sets to segment the plaque, which yielded high accuracy and repeatability. Initialization of the algorithm required the observer to choose anchor points on each boundary on a set of transverse slices. The lumen–intima boundary was segmented by constraining its evolution using the already segmented surface of the media–adventitia boundary, in addition to the global region-based information and the anchor points. Gill et al. [26] used a dynamic balloon model represented by a triangulated mesh, which was manually placed, for the segmentation of atherosclerotic plaque in 3D images (error = 0.3 mm between the manual and automated segmentations).

We present in Fig. 2c a normalized despeckled ultrasound image of the CCA from a symptomatic subject aged 63, with an atherosclerotic carotid plaque at the far wall and manual delineation from the expert of the plaque, IMC (IMT$_{mean}$ = 0.91 mm), and the near wall segmentation. In Fig. 2d, we present the complete automated segmentation of the CCA on the normalized despeckled ultrasound image from Fig. 2c, (IMT$_{mean}$ = 0.936 mm). The automated segmentation was performed by the system proposed in [49].

4.4 Atherosclerotic carotid plaque video segmentation techniques

Table 4 presents only two different studies [19, 58] that were found in the literature for the ultrasound video segmentation of the atherosclerotic carotid plaque. In [58], an integrated segmentation system for the segmentation of atherosclerotic carotid plaque in ultrasound video based on

snakes was introduced, whereas in [19], a Bayesian model based on motion estimation was proposed.

Figure 4 presents an example of video plaque segmentation with a large plaque appearing at the CCA at the 50th, 60th, 70th, and 150th normalized despeckled video frames of the video, respectively. It is the case of a 64-year-old male symptomatic subject, with a stenosis of 50–60 % and a stent on the right CCA. More specifically, we have the manual (left column) and the automated (right column) video segmentations of the CCA for the plaque and carotid diameter, in (a) 50th, (b) 60th, (c) 70th, and (d) 150th video frames of the video, respectively.

4.5 Integrated CCA image segmentation systems

There is only one study in the literature [56] that proposes an integrated system for the complete segmentation of the CCA bifurcation in ultrasound images. The CCA bifurcation is sequentially segmented into different distinct areas namely the IMC, lumen diameter, and the atherosclerotic carotid plaque. The system was based on image intensity normalization, despeckle filtering, initial contour estimation, and morphology segmentation prior to the application of the snakes segmentation algorithm. Furthermore, user interaction and manual corrections were possible. The algorithm was evaluated on 20 longitudinal ultrasound images of the CCA bifurcation with manual segmentations available from a neurovascular expert. The manual mean $\pm$ std measurements were for the IMT: (0.96 ± 0.22) mm, lumen diameter: (5.59 ± 0.84) mm, and internal carotid artery origin stenosis (48.1 ± 11.52) %, while the automated measurements were for the IMT: (0.93 ± 0.22) mm, lumen diameter: (5.77 ± 0.99) mm, and internal carotid artery stenosis (51.05 ± 14.51) %, respectively. We also found a true-positive fraction, TPF = (95.2 ± 7.1) %, a true-negative fraction, TNF = (98.1 ± 6.3) %, a Williams index, KI = 86 %, an overlap index, O = 79.3 %, specificity, Sp = 0.98, and a precision, P = 0.945 %. No significant differences were found between all manual and the automated segmentation measurements.

4.6 Diastolic and systolic states of the CCA

In Fig. 5, we illustrate an M-mode generation procedure as proposed in [52, 54, 58]. Figure 5a presents the first normalized and despeckled (with DsFlsmv) frame of a B-mode ultrasound video of the CCA, while Fig. 5b shows the segmentation of the plaque boundaries and the near wall of the CCA by snakes. The video was acquired from a symptomatic male subject aged 66. In Fig. 5c, we show the extracted CCA plaque, while in Fig. 5d, the despeckled M-mode image generated from the CCA video for a selected perpendicular B-mode line (shown in the left upper side of Fig. 5d). Figure 5e presents the initial

Manual Segmentations   Snakes based Segmentations
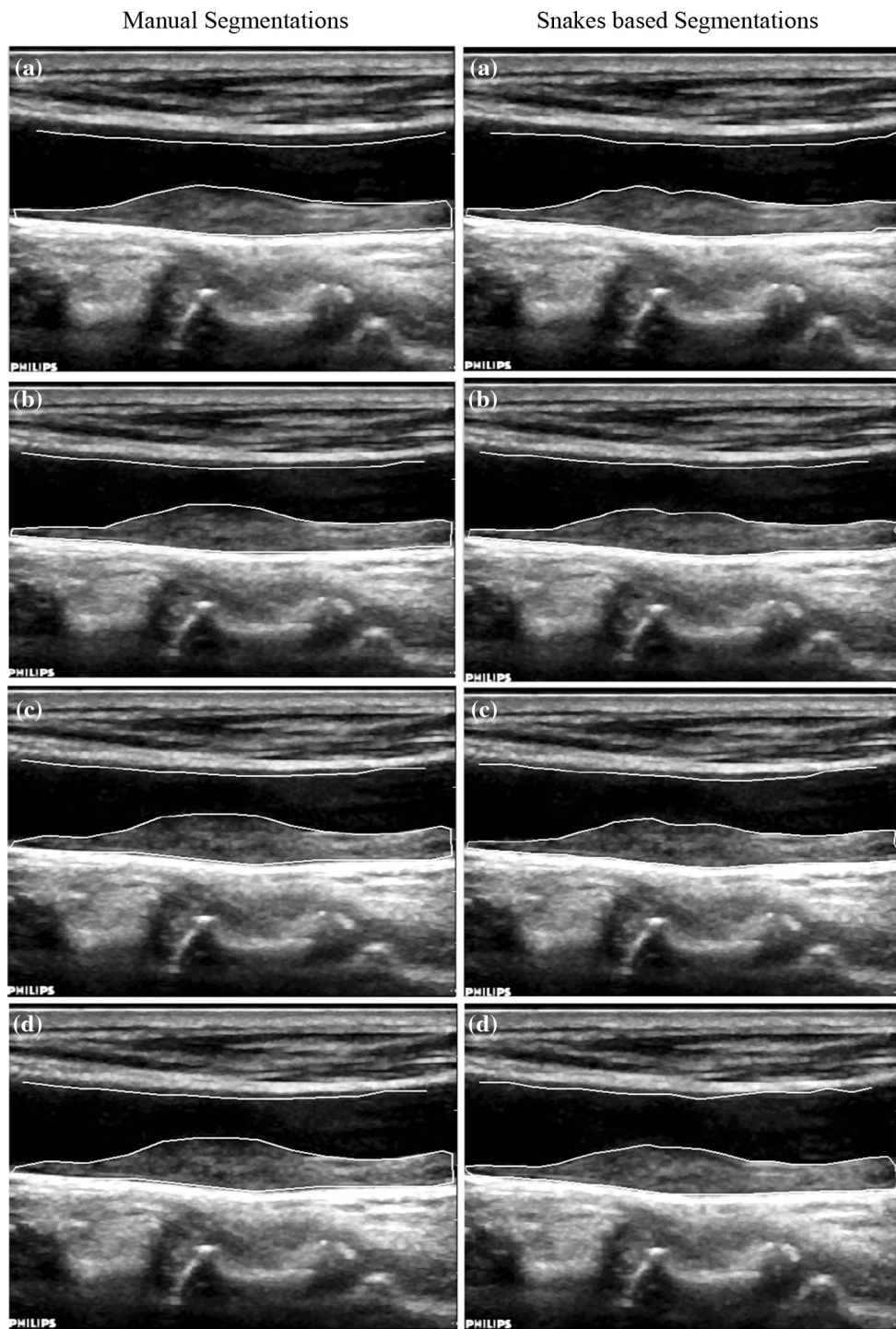
Fig. 4 Manual (*left column*) and automated (*right column*) video segmentation of the CCA [58] for the plaque and the carotid diameter, at the **a** 50th (IMT_{man} = 0.85 mm, $diameter_{man}$ = 6.69 mm, IMT = 0.99 mm, diameter = 6.9 mm), **b** 60th (IMT_{man} = 0.90 mm, $diameter_{man}$ = 7.31 mm, IMT = 0.93 mm, diameter = 7.51 mm), **c** 70th (IMT_{man} = 0.92 mm, $diameter_{man}$ = 6.98 mm, IMT = 0.95 mm, diameter = 7.21 mm), and **d** 150th (IMT_{man} = 0.90 mm, $diameter_{man}$ = 7.11 mm, IMT = 0.93 mm, diameter = 7.31 mm) normalized despeckled video frames of the video

M-mode diastolic and systolic artery states superimposed on the original M-mode image at the far and near walls, respectively. Finally, in Fig. 5f, we show the CCA diameter change with step diagram and systolic and diastolic frames of the video with maximum carotid diameter during distension (*) and maximum carotid diameter during contraction.

5 Discussion

Accurate and precise CCA segmentation in ultrasound imaging and video is imperative for evaluating and following up the risk of stroke in asymptomatic or symptomatic patients at risk of atherosclerosis. We have presented in this review paper the most widely used techniques for the segmentation of the CCA in ultrasound images and videos, which are summarized in Tables 1, 2, 3, 4. Those are usually presented as integrated software systems and are either semi or fully automated.

As shown in Table 1, a large number of segmentation techniques have been developed for the segmentation of the IMC in CCA ultrasound images. The best performing method in terms of the error between the manual and the automated IMT measurements may have an IMT bias lower than (0.001 ± 0.035) mm [23], followed by -0.005 mm [25] and (0.008 ± 0.02) mm [50], whereas the average error bias for the most automated techniques presented in Table 1 is lower than 10 μm. In terms of the number of images processed, the recent study by Destrempes et al. [18] outperforms the rest of the methods, followed by Molinari et al. [67], Delsanto et al. [17], Faita et al. [23], and Loizou et al. [48, 50]. In the majority of the proposed techniques, a one or two evaluation metrics were used to evaluate the segmentation method with the exception of [48] and [50], where additional metrics were employed. Finally, the higher degree of automation with less user interaction (see column UI in Table 1) is given by the methods [6, 35, 62, 67, 83, 106, 110]. In a recent review study performed on IMT segmentation techniques for CCA ultrasound imaging [65], it was shown that the best performing studies in terms of the MAD as well as the measurement errors were in [48, 50, 67], whereas in [17], a low IMT measurement error was demonstrated, but the technique in [17] avails a lower degree of automation.

The degree of user interaction is still crucial to obtain optimal IMT measurement performance. In a review study [70], on CCA IMT ultrasound image segmentation techniques, nine different segmentation studies were compared. The authors conclude that none of the existing techniques was superior in all aspects and recognized the need for further investigation on adaptive IMC segmentation techniques, which will provide higher accuracy, robustness, automation, and reduced processing time. In another study [109], the authors discussed a few commonly used methods for IMT segmentation and measurements. Furthermore, in [6], the authors presented a frequency domain implementation of active contours method, aiming to reduce the inter-observer variability and the subjectivity of the IMT measurements in a number of images. They found a maximum deviation of 3.4 pixels (0.0248 mm) for the IMT when compared to the manual tracings. In [25], IMT measurements were performed on 43 subjects using a software tool incorporated on a commercialized ultrasound scanner. It was found that the average time span for manual versus automated ($-/-$) measurements was 57.3 s/2.52 s, the CV % was 5.54 %/6.34 %, and the absolute difference 0.1 mm/0.05 mm, respectively. The inter-observer error showed no systematic error, while the variation and the repeatability coefficients were better for the automated than the manual measurements. Finally, in [65] and [86], a review of segmentation techniques for ultrasound image segmentation was presented. It should be furthermore noted that a number of other studies were reported in the literature with results for the manual or automated segmentation of the IMC, which are not presented in Table 1 and are here below shortly presented. More specifically, in [4], IMT was assessed on 126 ultrasound images using the QLAB software with 0.547 ± 0.095 mm, and 0.524 ± 0.068 mm of manual and the automated segmentation measurements. The bias between the two measurements was 0.023 ± 0.052 mm. Inter- and intra-observer coefficients were greater for the automated system (0.94 and 0.99 vs 0.72 and 0.88). A morphology contrast-based CCA lumen segmentation method taking into consideration the characteristics of the CCA lumen was presented in [89].

Table 2 shows that only very few semi-automated techniques have been developed so far for the ultrasound video segmentation of the IMC. Moreover, the best performing video IMC segmentation method in terms of the error between the manual and the automated IMT measurements has an IMT bias lower than (0.007 ± 0.176) mm [36], followed by (0.008 ± 0.02) mm [54]. It is also shown that the average error is lower when compared to the errors reported for the image segmentation of the IMC (see Table 1). The videos that were investigated were 82 [112], 40 [36], 10 [54], and 3 [11], respectively, whereas in [54], additional performance metrics were used for the evaluation of the segmentation method. The best automation is so far given by the study in [54]. More specifically in [54], the authors proposed and evaluated an integrated system for the segmentation of IMC and the lumen diameter in longitudinal ultrasound videos of the CCA. The method was based on frame normalization, speckle reduction filtering (DsFlsmv), and snakes segmentation. The algorithm was initialized in the first video frame of the cardiac cycle, by an automated initialization procedure, and the borders of the far wall and near wall of the CCA were estimated. The IMC and the carotid diameter were then segmented automatically in the consecutive video frames for one cardiac cycle. The algorithm was evaluated on 10 longitudinal ultrasound B-mode videos of the CCA and was compared with the manual tracings of a neurovascular expert, for every 20 frames in a time span of 3–5 s, covering in general 1–2 cardiac cycles. The algorithm estimated an $\text{IMT}_{\text{mean} \pm \text{standard deviation}}$ of 0.72 ± 0.22 mm, while the manual results
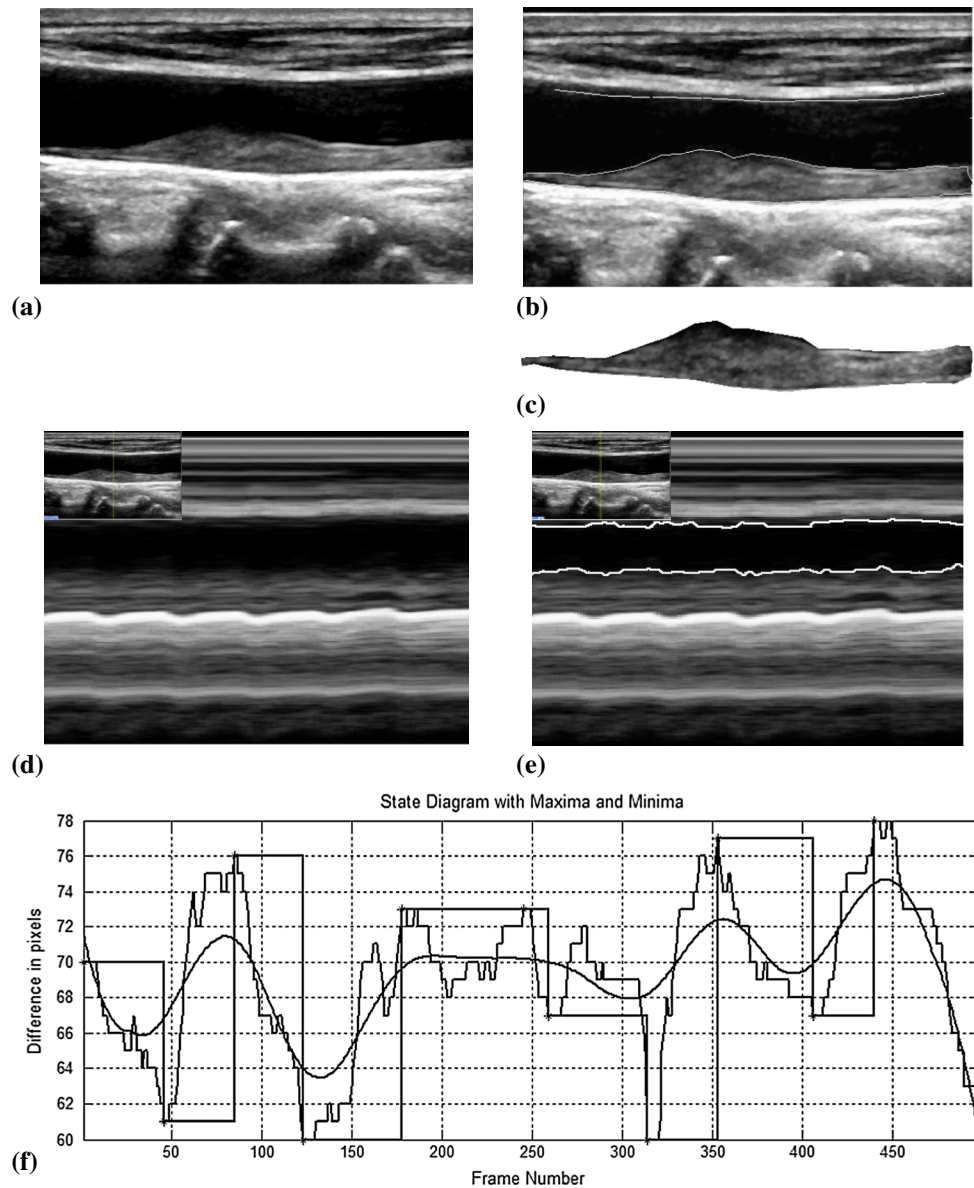
Fig. 5 Illustration of the M-mode procedure (see [58] for the implementation details), **a** first normalized and despeckled (with *DsFlsmv*) frame of a B-mode ultrasound video of the CCA, **b** segmentation of the plaque boundaries and the near wall of the CCA by snakes, **c** extracted plaque, **d** despeckled M-mode image generated from the CCA video for a selected B-mode line, **e** initial M-mode states superimposed on the original M-mode image at the far and near walls, respectively, **f** CCA diameter change averaged across the major plaque axis quintiles, with step diagram and systolic and diastolic frames of the video with maximum carotid diameter during distension (*asterisk*) and maximum carotid diameter during contraction. Diastolic and systolic frames (from 0 to 460) (100 frames per second = 4.6 s). Contraction frames: 46, 123, 259, 314, 406. Distension Frames: 1, 85, 178, 245, 353, 440. Minimum Carotid Diameter: 3.52 mm at frame 123. Maximum Carotid Diameter: 3.89 mm at frame 440

were 0.70 ± 0.19 mm. The mean maximum and minimum diameter was 7.08 ± 1.37 mm and 6.53 ± 1.13 mm, respectively. The results were validated based on statistical measures univariate statistical analysis and manual observers' delineations. It was found that there was no significant difference between the snakes segmentation measurements and the manual measurements. The integrated system proposed in [54] could thus successfully segment the IMC in

ultrasound CCA video sequences complementing manual measurements.

Table 3 presents, an overview of plaque segmentation techniques in ultrasound images of the CCA. There we may observe that the best performing technique in terms of the number of images is the study by Loizou et al. [49], followed by [12, 17, 28, 79, 100, 111]. In terms of the TPF, the best method is the level sets-based segmentation

study prosed by Golemati et al. [28], followed by [111], [100], [12], and then by [49], with a TRF of 97.5 ± 1.0 %, 96.7 ± 1.7 %, 95 %, 94.4 ± 2.2 %, and 82.70 ± 2.1 %, respectively. Additional evaluation metrics were employed in [49]. The degree of automation is very high for the techniques in [49, 111]. Some of the methods reported in Table 3 were also reviewed in [4] and [42]. In another study [78], a segmentation method based on Nakagami distributions was proposed for classifying plaque pixels into a fixed number of components. The method was able to successfully distinguish asymptomatic from symptomatic patients.

Table 4 illustrates only two different plaque segmentation techniques [19, 58] that have been very recently proposed for the video segmentation of the atherosclerotic carotid plaque in ultrasound videos of the CCA. The number of videos investigated was 43 and 33, respectively. The Bayesian model-based segmentation method by Destrempes et al. [19] gave the best TNF [TNF = (83.7 ± 8.3) %] followed by the snakes-based segmentation method proposed by Loizou et al. [58] [TNF = (84.3 ± 7.5) %]. The method presented in [58] integrates video frames normalization, despeckling, and segmentation using active contours. Similar metrics were used for the evaluation of the segmentation techniques in both the above studies, where the snakes-based segmentation technique [58] (9 s) outperformed the Bayesian model based [19] (30 s) on terms of segmentation time. The best degree of automation is given by the technique in [19].

Finally, there is only one study in the literature [56] that proposes an automated segmentation system for the complete segmentation of the CCA bifurcation in ultrasound images based on snakes. No significant differences between all manual and the automated segmentation measurements were found in [56].

A number of limitations for the segmentation of the CCA from ultrasound images and videos include cases of atherosclerotic plaque types I and IV [21, 58, 95], which should not be included in the studies for segmentation. Different protocols are used for each study, but there are also problems due to differences in anatomy, as well as the extent of the atherosclerosis and plaque presence, which should be taken into consideration. The presence of extensive and severe carotid stenosis may cause the initialization of the algorithm to completely fail as there will be difficulty in establishing the lumen of the CCA. In addition, the presence of extensive plaques in the near wall may cause inaccurate segmentation of the far wall adventitia. It should be noted that the parameters for each processing step should be selected for maximum performance (for example, the size of the moving pixel window, the number of iterations, the number of frames for which the contour is or re-initialized in the case of video segmentation). The average computational time for some techniques is still very high,

and this causes difficulties in their application in the real clinical practice. A complete discussion on additional limitations of the methods can also be found in [52]–[49], [56], [62]–[57], [5]–[111], [18, 67]. Finally, in order to handle the variability caused by different datasets, we have started working toward the creation of standard image and video datasets with ground truth (which can be downloaded from http://www.medinfo.cs.ucy.ac.cy). Prior work in this direction was carried out by Mollinary et al. [68], who used the ultrasound images for the segmentation of intima–media complex (not covering plaque segmentation of the CCA). The creation and use of a standard dataset will ensure high accuracy of the segmentation results when other researchers apply their techniques on the same standard data set of images/videos, thus having a common platform for comparing their segmentation performance. It should be furthermore noted that most of the CCA segmentation systems, presented in this review (see Tables 1, 2, 3, 4), are able to be calibrated manually by the user of the system before the segmentation of the structure of interest. This is usually done manually by the user, in order to overcome difficulties arising from different datasets. The calibration procedure will estimate the actual pixel size in millimeters from the image (using a conversion factor) so that the correct distance of the structure of interest can be calculated.

In general, snake segmentation techniques, which are conducted mainly under human supervision, exhibit better segmentation measurement performance than the others. The IMT or the plaque is usually measured in a small selected image area (ROI) where there is good visibility of the structures of interest. The user may interact with the segmentation process and increase the measurement performance. The rest of the segmentation techniques do not focus on a small ROI, but they generally operate on the whole image. One possible enhancement is to adopt an intelligent strategy for reducing the image to an ROI in which the IMT or plaque can be segmented. Neural networks, fuzzy logic, and trained classifiers could all help in this direction. The disadvantage of such an approach would be the higher computational cost and that measurements cannot be performed in real time. Another major advantage of the non-snake segmentation techniques is their ability to process large amounts of data and be robust with respect to image characteristics. Furthermore, they can better handle difficulties in image and vessel morphology (i.e., straight, curved, inclined, and vessels with plaques can all be processed).

Further efficiency can be achieved on commercial software versions, while the algorithms may also be designed to perform parallel with the clinician's evaluation so that the clinician might carry on the patient examination, while the segmentation of the structure is performed. Thus, there is a reasonable expectation to create clinically applicable

versions in the future especially for the video segmentation of the IMC and plaques in the CCA. Another possible solution is to merge different segmentation techniques and apply them on selected image areas (i.e., intima, adventitia, lumen, plague, and CCA bulb.) where best performance is demonstrated. It should be furthermore noted that a direct comparison of IMT and plaque segmentation measurements is difficult to be made due to the difference in axial resolution of the ultrasound scanner used in each study.

Future research will incorporate the extraction of texture features [33], from the IMC and the atherosclerotic carotid plaque, from ultrasound images and or videos. Those features may be used to separate subjects in high and low-stroke-risk groups, as was also shown in [51] and [53]. More specifically, in [51], texture features, whereas in [53], amplitude-modulation frequency-modulation features were extracted from the IMC, which have been used to separate asymptomatic and symptomatic subjects, as well as to classify the subjects in different age-groups. However, a larger-scale study is required for evaluating the systems before their application in the real praxis, which requires integrated software applications for image [59] and video [57] despeckle filtering.

6 Concluding remarks and future directions

We have presented the most widely used techniques for the segmentation of the CCA IMT and the atherosclerotic carotid plaque from ultrasound images and videos. The trend is now toward the complete automation carotid IMT measurements, which will assist the clinician in the clinical practice. As this review shows, there is still no sufficient overall system performance demonstrated for the automated systems, for the segmentation of the IMC or plaque in the CCA either with images or with videos. We have also shown that the overall performance of the semi-automated systems is higher when compared to the performance of the automated segmentation systems. We illustrate in Table 1 that the best performing IMC segmentation system may have and IMT error of about 1×10^{-3} mm [23], where on average the best performing systems have a bias of around 50×10^{-3} mm [45, 48, 92, 103, 108]. The best performing IMC video segmentation method was proposed in [36] (see Table 2), while the best plaque image segmentation method was proposed in [28] (see Table 3). The best method for the IMC video segmentation was proposed in [19] (see Table 4), while an integrated segmentation method for the complete image segmentation of the CCA was proposed in [56].

With the rapidly growing development of new CCA segmentation methods, it is expected that the performance of the automated methods will be further increased and can be soon comparable with semi-automated segmentation techniques. Further improvement on the performance and accuracy of the segmentation methods will also increase the performance of automated classification in ultrasound plaque images [14] as well as the identification of groups of patients [51, 53]. It is furthermore expected that 3D carotid imaging will be used for monitoring carotid atherosclerosis progression and regression, where new 3D techniques should be developed in order to be applied routinely in the clinical practice, where the segmentation of plaque lumen and vessel is of utmost importance. Furthermore, improved 3D segmentation techniques will accelerate the segmentation process and the evaluation of the disease and provide visual evidence of spatial and temporal dynamics of carotid artery changes in response to therapy [40]. It will also be interesting to use the above segmentation techniques for detecting artery calcifications in carotid plaques as it was shown in [115]. The correct identification and measurement of those calcifications may be helpful in estimating the depth and circumferential extent of calcifications, the type of interventional devices, and the risk of complications. The current research will also be helpful in advancing the area of motion estimation when working with clinical videos. The video segmentations of the atherosclerotic carotid plaque [58] may be used in order to estimate accurate velocities of clinical videos [69], which will show normal or abnormal motion. Furthermore, accurate segmentation in video will facilitate the correct monitoring of the wall and plaque changes, as well as the characteristics of the arterial wall in the CCA and its elasticity [52], which may have significant clinical relevance for the assessment of future CVD events.

References

1. Abdel-Dayen AR, El-Sakka MR (2004) A novel morphological-based carotid artery contour extraction. Proc Can Conf Electr Comput Eng 4:1873–1876
2. Abolmaesumi P, Sirouspour MR, Salcudean SE (2000) Real-time extraction of carotid artery contours from ultrasound images. Proc. IEEE Int Conf Computer Based Medical Systems, p 181–186
3. ACAS clinical advisory (1994) Carotid endarterectomy for patients with asymptomatic internal carotid artery stenosis. Stroke 25(12):2523–2524
4. Ananey OM, Mellotte G, Maher V (2014) Comparison of semi-automated and manual measurements of carotid intima-media thickening. Bio Med Res Int 2014:1–4
5. Bartels S, Franco AR, Rundek T (2012) Carotid intima-media thickness (cIMT) and plaque from risk assessment and clinical use to genetic discoveries. Perspect Med 1(1–12):139–145
6. Bastida-Jumilla MC, Mechon-Lara RM, Morales-Sanchez J, Verdu-Monedero R et al (2013) Segmentation of the common carotid artery walls based on a frequency implementation of active contours. J Digit Imaging 26(1):129–139

7. Bland JM, Altman DG (1986) Statistical methods for assessing agreement between two methods of clinical measurement. Lancet 1(8476):307–310

8. Bots ML, Hoes AW, Koudstaal PJ, Hofman A, Grobbee DE (1997) Common carotid intima-media thickness and risk of stroke and myocardial infarction: the Rotterdam Study. Circulation 96:1432–1437

9. Chalana V, Kim Y (1997) A methodology for evaluation of boundary detection algorithms on medical images. IEEE Trans Med Imag 16(5):642–652

10. Cheng D, Schmidt-Trucksaess A, Cheng K, Burkhardt H (2002) Using snakes to detect the intimal and adventitial layers of the common carotid artery wall in sonographic images. Comput Meth Prog Biomed 67:27–37

11. Cheng D-C, Schmidt-Trucksaess A, Liu C-H, Liu S-H (2010) Automated detection of the arterial walls of the common carotid artery based on dynamic B-mode signals. Sensors 10:10601–10619

12. Cheng J, Li H, Fenster A, Zhang X, He X, Ding M (2013) Fully automatic plaque segmentation in 3D ultrasound images. Ultrasound Med Biol 39(2):2431–2446

13. Chiu B, Ukwatta E, Shavakh S, Fenster A (2013) Quantification and visualisation of carotid segmentation accuracy and precision using a 2D standardised carotid map. Phys Med Biol 58:3671–3703

14. Christodoulou CI, Pattichis CS, Pantziaris M, Nicolaides AN (2003) Texture-based classification of atherosclerotic carotid plaques. IEEE Trans Med Imag 22(7):902–912

15. Cohen LD (1991) On active contour models and balloons. Comput Vis Graph Image Process Image Underst 53(2):211–218

16. Cohen I, Cohen LD, Ayache N (1992) Using deformable surfaces to segment 3-D images and inter differential structures. CVGIP Image Underst 56(2):242–263

17. Delsanto S, Mollinari F, Giustetto P, Liboni W, Badalamenti S, Suri JS (2007) Characterization of a completely user-independent algorithm for carotid artery segmentation in 2-D ultrasound images. IEEE Trans Instrum Meas 56(4):1265–1274

18. Destrempes F, Meunier J, Giroux M-F, Soulez G, Cloutier G (2009) Segmentation in ultrasound B-mode images of healthy carotid arteries using mixtures of Nakagami distributions and stochastic optimization. IEEE Trans Med Imag 28(2):215–229

19. Destrempes F, Meunier J, M-F Giroux, Soulez G, Cloutier G (2011) Segmentation of plaques in sequences of ultrasonic B-mode images of carotid arteries based on motion estimation and a Bayesian model. IEEE Trans Biomed Eng 58(8):2202–2211

20. Dutt V (1995) Statistical analysis of ultrasound echo envelope. Ph.D. dissertation, Mayo Graduate School, Rochester, MN

21. Elatrozy T, Nicolaides AN, Tegos T, Zarka A, Griffin M, Sabetai M (1998) The Effect of B-mode ultrasonic image standardization of the echodensity of symptomatic and asymptomatic carotid bifurcation plaque. Int Angiol 17(3):179–186

22. Executive Committee for the Asymptomatic Carotid Atherosclerosis study (2002) Endarterectomy for asymptomatic carotid stenosis. J Am Med Assoc 273:1421–1428

23. Faita F, Gemignani V, Bianchini E, Giannarelli C, Ghiadoni L, Demi M (2008) Real-time measurement system for evaluation of the carotid intima-media thickness with a robust edge operator. J Ultrasound Med 27(9):1353–1361

24. Fleiss JL, Cohen J, Everitt BS (1969) Large sample standard errors of kappa and weighted kappa. Psychol Bull 72(5):323–327

25. Freire CMV, Ribeiro ALP, Barbosa FBL, Nogueira AI et al (2009) Comparison between automated and manual measurements of carotid intima-media thickness in clinical practice. Vasc Health Risk Manage 5:811–817

26. Gill JD, Ladak HM, Steinman DA, Fenster A (2000) Segmentation of ulcerated plaque: a semi-automatic method for tracking the progression of carotid atherosclerosis. World congress Med Phys Biomed Eng Chicago, IL, pp 1–4

27. Go AS, Mozaffarian D, Veronique LR, Benjamin EJ et al (2013) Heart disease and stroke statistics-2013 update: a report from the American Heart Association. Circulation 127:e6–e245

28. Golemati S, Stoitsis J, Sifakis EM, Balkizas T, Nikita K (2007) Using the Hough transform to segment images of longitudinal and transverse sections of the carotid artery. Ultrasound Med Biol 33(12):1918–1932

29. Guerrero J, Salcudean SE, McEwen JA, Masri BA, Nicolaou S (2007) Real-time vessel segmentation and tracking for ultrasound imaging applications. IEEE Trans Med Imag 26(8):1079–1090

30. Gutierrez M, Pilon P, Lage S, Kopel L, Carvalho R, Furuie S (2002) Automatic measurement of carotid diameter and wall thickness in ultrasound images. Comput Cardiol 29:359–362

31. Halenka M (1999) Noninvasive measurement of early atherosclerosis by high-resolution B-mode ultrasonography. Acta Universitatis Palackianae Olomucensis Facultatis Medicae 142:7–11

32. Hamou AK, El-Sakka MR (2004) A novel segmentation technique for carotid ultrasound image. Proc Int Conf Acoust Speech Signal Process III:521–524

33. Haralick RM, Shanmugam K, Dinstein I (1973) Texture features for image classification. IEEE Trans Syst Man Cyb SMC 3(6):610–621

34. Huang C-C, Chen T, Chao T-H, Juan Y-F (2004) The investigation of the relationship between carotid intima-media thickness and vascular compliance in patients with coronary artery disease. Biomed Eng 16(1):37–42

35. Ilea DE, Whelan PF, Brown C, Stanton A (2009) An automatic 2D CAD algorithm for the segmentation of the IMT in ultrasound carotid artery images. Proc 31st Int Conf IEEE Eng Med Biol Soc: Engin the Future of Biomed, pp 515–519

36. Illea DE, Duffy C, Kavanagh L, Stanton A, Whelan PF (2013) Fully automated segmentation and tracking of the intima media thickness in ultrasound video sequences of the common carotid artery. IEEE Trans Ultrason Ferroelectr Freq Control 60(1):158–177

37. Järvisalo MJ, Putto-Laurila A, Jartti L, Lehtimaeki T et al (2002) Carotid artery intima-media thickness in children with type 1 diabetes. Diabetes 51(2):493–498

38. Kakisis JD, Avgerinos ED, Antonopoulos CN, Giannakopoulos TG, Moulakalis K, Liapis CD (2012) The European society of vascular surgery guidelines for carotid intervention: an updated independent assessment and literature review. Eur J Vasc Endovasc Surg 44(3):238–243

39. Kass M, Witkin A, Terzopoulos D (1998) Snake: active contour models. Int J Comput Vision 1:321–331

40. Krasinksi A, Chiu B, Spence JD, Fenster A, Parraga G (2009) Three-dimensional ultrasound quantification of intense statin treatment of carotid atherosclerosis. Ultrasound Med Biol 35(11):1763–1772

41. Kyriakou E, Pattichis MS, Christodoulou C, Pattichis CS, Kakkos S, Griffin M, Nicoliades AN (2005) Ultrasound imaging in the analysis of carotid plaque morphology for the assessment of stroke. In: Suri JS, Yuan C, Wilson DL, Laxminarayan S (eds) Plaque imaging: pixel to molecular level. IOS press, Amsterdam, pp 241–275

42. Kyriakou E, Pattichis CS, Pattichis MS, Loizou CP, Christodoulou C, Kakkos SK, Nicolaides AN (2010) A review of non-invasive ultrasound image processing methods in the analysis of carotid plaque morphology for the assessment of stroke risk. IEEE Trans Inf Techn Biomed 14(4):1027–1038

43. Lamont D, Parker L, White M, Unwin N et al (2000) Risk of cardiovascular disease measured by carotid intima-media thickness at age 49-51: life course study. BMJ 320(7230):273–278

44. Lee J-S (1980) Digital image enhancement and noise filtering by use of local statistics. IEEE Trans Pattern Anal Mach Intell 2:165–168

45. Liang Q, Wendelhag I, Wilkstrand J, Gustavsson T (2000) A multiscale dynamic programming procedure for boundary detection in ultrasonic artery images. IEEE Trans Med Imag 19(2):127–142

46. Loizou CP, Pattichis CS, Christodoulou CI, Istepanian RSH, Pantziaris M, Nicolaides AN (2005) Comparative evaluation of despeckle filtering in ultrasound imaging of the carotid artery. IEEE Trans Ultrason Ferroelectr Freq Contr 52(10):1653–1669

47. Loizou CP, Pattichis CS, Pantziaris M, Tyllis T, Nicolaides AN (2006) Quantitative quality evaluation of ultrasound imaging in the carotid artery. Med Biol Eng Comput 44(5):414–426

48. Loizou CP, Pattichis CS, Pantziaris M, Tyllis T, Nicolaides AN (2007) Snakes based segmentation of the common carotid artery intima media. Med Biol Eng Comput 45(1):35–49

49. Loizou CP, Pattichis CS, Pantziaris M, Nicolaides AN (2007) An integrated system for the segmentation of atherosclerotic carotid plaque. IEEE Trans Inf Technol Biomed 11(6):661–667

50. Loizou CP, Pattichis CS, Nicolaides AN, Pantziaris M (2009) Manual and automated media and intima thickness measurements of the common carotid artery. IEEE Trans Ultras Ferroel Freq Contr 56(5):983–994

51. Loizou CP, Pantziaris M, Pattichis MS, Kyriakou E, Pattichis CS (2009) Ultrasound image texture analysis of the intima and media layers of the common carotid artery and its correlation with age and gender. Comput Med Imag Graph 33(4):317–324

52. Loizou CP, Pantziaris M, Pattichis CS, Kyriakou E (2010) M-mode state-based identification in ultrasound videos of the common carotid artery. In: Proceeding 4th International Symposium on Communication, Control and Signal Processing, ISCCSP, Limassol, Cyprus, March 3–5, p 6

53. Loizou CP, Murray V, Pattichis MS, Pantziaris M, Pattichis CS (2011) Multiscale Amplitude modulation-Frequency Modulation (AM-FM) texture analysis of ultrasound images of the intima and media layers of the carotid artery. IEEE Trans Inf Tech Biomed 15(2):178–188

54. Loizou CP, Kasparis T, Papakyriakou P, Christodoulou L, Pantziaris M, Pattichis CS (2012) Video segmentation of the common carotid artery intima media complex. IEEE 12th Int Conf Bioinf and Bioeng (BIBE), Cyprus, pp. 500–505

55. Loizou CP, Kasparis T, Christodoulides P, Theofanous C, Pantziaris M, Kyriakou E, Pattichis CS (2012) Despeckle filtering in ultrasound video of the common carotid artery, 12th Int Conf Bioinformatics Bioengineering Proc (BIBE), Cyprus, Nov 11–13, p 4

56. Loizou CP, Kasparis T, Spyrou C, Pantziaris M (2013) Integrated system for the complete segmentation of the carotid artery bifurcation in ultrasound images. IFIP Int Federation Inform Proc, 9th Int Conf Artific Intellig Applic & Innov (AIAI 2013) IFIP AICT 412, Cyprus, 26–28 Sept, pp. 292–301

57. Loizou CP, Theofanous C, Pantziaris M, Kasparis T, Christodoulides P, Nicolaides AN, Pattichis CS (2013) Despeckle filtering toolbox for medical ultrasound video. Int J Monit Surveill Technol Res (IJMSTR) 4(1):61–79

58. Loizou CP, Petroudi S, Pattichis CS, Pantziaris M, Nicolaides AN (2014) An integrated system for the segmentation of atherosclerotic carotid plaque in ultrasound video. IEEE Trans Ultras Ferroel Freq Contr 61(1):86–101

59. Loizou CP, Theofanous C, Pantziaris M, Kasparis T (2014) Despeckle filtering software toolbox for ultrasound imaging of the common carotid artery. Comput Methods Prog Biomed 114:109–124

60. Mancini GBJ, Abbott D, Kamimura C, Yeoh E (2004) Validation of a new ultrasound method for the measurement of carotid artery intima medial thickness and plaque dimensions. Can J Cardiol 20(13):1355–1359

61. Mao F, Gill J, Downey D, Fenster A (2000) Segmentation of carotid artery in ultrasound images: Method development and evaluation technique. Med Phys 27(8):1–10

62. Mechon-Lara RM, Bastida-Jumila MC, Morales-Sanchez J, Sancho-Gomez JL (2014) Automatic detection of the intima-media thickness in ultrasound images of the common carotid artery using neural networks. Med Biol Eng Comput 52(2):169–181

63. Metz C (1978) Basic principles of ROC analysis. Semin Nucl Med 8:283–298

64. Mojsilovic A, Popovic M, Amodaj N, Babic R, Ostojic M (1997) Automatic segmentation of intravascular ultrasound images: a texture based approach. Ann Biomed Eng 25(6):1059–1071

65. Molinari F, Zeng G, Suri JS (2010) A state of the art review on intima-media thickness (IMT) measurement and wall segmentation techniques for carotid ultrasound. Comput Method Prog Biomed 100:201–221

66. Molinari F, Meiburger KM, Saba L, Acharya UR, Ledda M, Nicolaides AN, Suri JS (2012) Constrained snake vs. conventional snake for carotid ultrasound automated IMT measurements on multi-center data sets. Ultrasonics 52:949–961

67. Molinari F, Pattichis C, Zeng G, Saba L et al (2012) Completely automated multi-resolution edge snapper. A new technique for an accurate carotid ultrasound IMT measurement: clinical validation and benchmarking on a multi-institutional database. IEEE Trans Image Process 21:1211–1222

68. Mollinari F, Zeng G, Suri JS (2010) An integrated approach to computer based automated tracings and its validation for 200 common carotid artery wall ultrasound images. J Ultras Med 29:399–418

69. Murillo S, Pattichis MS, Soliz P, Loizou CP, Pattichis CS (2010) Global optimization for motion estimation with applications to ultrasound videos of carotid artery plaques. SPIE Medical Imaging, San Diego, California, pp 7629–7632

70. Naik V, Gamad RS, Bansod PP (2013) Carotid artery segmentation in ultrasound images and measurement of intima-media thickness. Biomed Research Int 801962:1–10

71. Nicolaides AN, Sabetai M, Kakkos SK, Dhanjil S, Tegos T, Stevens JM (2003) The asymptomatic carotid stenosis and risk of stroke study. Int Angiol 22(3):263–272

72. O'Leary DH, Polak JF, Kronmal RA, Manolio TA, Burke GL, Wolfson SK Jr (1999) Carotid-artery intima and media thickness as a risk factor for myocardial infarction and stroke in older adults. New Engl J Med 340(1):14–22

73. Petroudi S, Loizou CP, Pantziaris M, Pattichis CS (2012) Segmentation of the common carotid intima-media complex in ultrasound images using active contours. IEEE Trans Biomed Eng 59(11):3060–3069

74. Pignoli P, Tremoli E, Poli A, Oreste P, Poaletti R (1986) Intima plus media thickness of the arterial wall: a direct measurement with ultrasound imaging. Atherosclerosis 74(6):1399–1406

75. Polak JF, Pencina MJ, Meisner A, Pencina KM, Brown LS, Wolf PA, D'Agostino RB Sr (2010) Associations of carotid artery intima-media thickness (IMT) with risk factors and prevalent cardiovascular disease: comparison of mean common carotid artery IMT with maximum internal carotid artery IMT. J Ultrasound Med 29(12):1759–1768

76. Polak JF, Funk LC, O'Leary DH (2011) Inter-reader differences in common carotid artery intima-media thickness: Implications

for cardiovascular risk assessment and vascular age determination. J Ultrasound Med 30(7):915–920

77. Polak JF, Pencina MJ, Herrington D, O'Leary DH (2011) Associations of edge-detected and manual-traced common carotid intima-media thickness measurements with Framingham risk factors: the multi-ethnic study of atherosclerosis. Stroke 42(7):1912–1916

78. Poree J, Destrembes F, Soulez G, Cloutier G (2011) Segmentation of atherosclerotic plaque components in ultrasound B-mode images using a multiphase Bayesian Level-set. IEEE Int Ultrason Symp, p 1391-1394

79. Rocha R, Campilho A, Silva J, Azevedo E, Santos R (2010) Segmentation of the carotid intima-media region in B-mode ultrasound images. Image Vis Comput 28(4):614–625

80. Rocha R, Silva J, Campilho A (2014) Automatic detection of the carotid lumen axis in B-mode Ultrasound images. Comput Methods Prog Biomed 15(3):110–118

81. Rosenfield GH, Fitzpatrick Lins K (1986) A coefficient of agreement as a measure of thematic classification accuracy. Photogramm Eng Remote Sens 52(2):223–227

82. Rossi AC, Brands PJ, Hoeks AP (2008) Automatic recognition of the common carotid artery in longitudinal ultrasound B-mode scans. Med Image Anal 12:653–665

83. Rossi AC, Brands PJ, Hoeks P (2010) Automatic localization of intimal and adventitial carotid artery layers with non-invasive ultrasound: a novel algorithm providing scan quality control. Ultrasound Med Biol 36(3):467–479

84. Rothwell PM, Gibson RJ, Slattery J, Warlow CP (1994) Prognostic value and reproducibility of measurements of carotid stenosis. A comparison of three methods on 1001 angiograms. European carotid surgery trialists' collaborative group. Stroke 25:2440–2444

85. Saba L, Molinari F, Meiburger KM, Piga M, Zeng G, Rajendra Achraya U, Nicolaides A, Suri JS (2012) What is the correct distance measurement metric when measuring carotid ultrasound intima-media thickness automatically? Int Angiol 31(5):483–489

86. Saini K, Dewal ML, Rohit M (2010) Ultrasound imaging and image segmentation in the area of ultrasound: a review. Int J Adv Sci Technol 24:41–60

87. Santhiyakumari N, Madheswran M (2009) Analysis of atherosclerosis for identification of cerebrovascular and cardiovascular diseases using active contour segmentation of carotid artery. Int J Bio Med Eng Consumer Health Inform 1(2):121–125

88. Santhiyakumari N, Rajendran P, Madheswaran M, Suresh S (2011) Detection of the intima and media layer thickness of ultrasound common carotid artery image using efficient active contour segmentation technique". Med Biol Eng Comput 49:1299–1310

89. Santos AMF, Dos Santos RM, Castro PMAC et al (2013) A novel automatic algorithm for the segmentation of the lumen of the carotid artery in ultrasound B-mode images. Expert Sys Appl 40(6570):6579

90. Selzer RH, Mack WJ, Lee PL, Kwong-Fu H, Hodis HN (2001) Improved common carotid elasticity and intima-media thickness measurements from computer analysis of sequential ultrasound frames. Atherosclerosis 154(1):185–193

91. Slabaugh G, Unal G, Wels M, Fang T, Rao B (2009) Statistical region based segmentation of ultrasound images. Ultrasound Med Biol 35(5):781–795

92. Stein JH, Korcarz CE, Mays ME, Douglas PS et al (2005) A semiautomated ultrasound border detection program that facilitates clinical measurement of ultrasound carotid intima-media thickness. J Am Soc Echocardiogr 18(3):244–251

93. Sundholm J, Gustavsson T, Sarkola T (2014) Semi-automated border detection software for the quantification of arterial lumen, intima-media and adventitia layer thickness with very-high resolution ultrasound. Atherosclerosis 234:283–287

94. Suri JS, Haralick RM, Sheehan FH (2000) Greedy algorithm for error correction in automatically produced boundaries from low contrast ventriculograms. Pattern Anal Appl 3(1):39–60

95. Tegos T, Sabetai M, Nicolaides AN, Elatrozy TS et al (2001) Patterns of brain computed tomography infraction and carotid plaque echogenicity. J Vasc Sur 33:334–339

96. Touboul PJ, Prati P, Scarabin P, Adrai V et al (1992) Use of monitoring software to improve the measurement of carotid wall thickness by B-mode imaging. J Hypertens 10(Suppl. 5):S37–S41

97. Touboul PJ, Vicaut E, Labreuche J, Belliard JP, Cohen S, Kownator S, Pithois-Merli I (2005) Design, baseline characteristics and carotid intima-media thickness reproducibility in the PARC study. Cerebrovasc Dis 19(1):57–63

98. Touboul PJ, Hernandez-Hernandez R, Kucukoglu S, Woo KS et al (2007) Carotid artery intima media thickness, plaque and Framingham cardiovascular score in Asia Africa/Middle East and Latin America: the PARC-AALA study. Int J Cardiovasc Imaging 23(5):557–567

99. Udupa JK, LeBlanc VR, Zhuge Y, Imielinska C et al (2006) A framework for evaluating image segmentation algorithms. Comput Med Imag Craph 30(2):75–87

100. Ukwatta E, Yuan J, Buchanan D, Chiu B et al (2013) Three-dimensional segmentation of three-dimensional ultrasound carotid atherosclerosis using sparse field level sets. Med Phys 40(5):1–17

101. van Der Meer IM, Bots ML, Hofman A, Del Sol AI, Van Der Kuip DAM, Witteman JCM (2004) Predictive value of non-invasive measures of atherosclerosis for incident myocardial infarction: the Rotterdam Study. Circulation 109(9):1089–1094

102. Wang J, Li X (2003) Guiding ziplock snakes with a priori information. IEEE Trans Image Process 12(2):176–185

103. Wendelhag I, Liang Q, Gustavsson T, Wikstrand J (1997) A new automated computerized analysing system simplifies reading and reduces the variability in ultrasound measurement of intima media thickness. Stroke 28:2195–2200

104. Wilhjelm JE, Gronholdt ML, Wiebe B, Jespersen SK, Hansen LK, Sillesen H (1998) Quantitative analysis of ultrasound B-mode images of carotid atherosclerotic plaque: correlation with visual classification and histological examination. IEEE Trans Med Imaging 17(6):910–922

105. Williams DJ, Shah M (1992) A fast algorithm for active contour and curvature estimation. GVCIP Imag Underst 55(1):14–26

106. Xiao G, Brady M, Noble JA, Zhang Y (2002) Segmentation of ultrasound B-mode images with intensity inhomogeneity correction. IEEE Trans Med Imaging 21(1):48–57

107. Xu C, Prince J (1997) Gradient vector flow: A new external force for snakes. IEEE Conf Comp Pattern Recogn (CVPR'97):66-71

108. Xu X, Zhou Y, Cheng X, Song E, Li G (2012) Ultrasound intima-media segmentation using Hough transform and dual snake model. Comp Med Imag Graph 36:248–258

109. Yang X (2012) A review on artery wall segmentation techniques and intima-media thickness measurements for carotid ultrasound images. J Innovative Optic Health Sci 5(1):1–10

110. Yang X, Jin J, Xu M, Wu H, He W, Yuchi M, Ding M (2013) Ultrasound common carotid artery segmentation based on active shape model. Comput Math Methods Med 2013:3459–3468

111. Zahalka A, Fenster A (2001) An automated segmentation method for three-dimensional carotid ultrasound images. Phys Med Biol 46:1321–1342

112. Zahnd G, Orkisz M, Sérusclat A, Moulin P, Vray D (2014) Simultaneous extraction of carotid artery intima-media

interfaces in ultrasound images: assessment of wall thickness temporal variation during the cardiac cycle. Int J CARS 9(4):645–658

113. Zarins CK, Xu C, Glagov S (2001) Atherosclerotic enlargement of the human abdominal aorta. Atherosclerosis 155(1):157–164

114. Zhang H, Fritts JE, Goldman AA (2008) Image segmentation evaluation: a survey of unsupervised methods. Coput Vis Image Underst 110:260–280

115. Zhang Q, Yuanyuan W, Weiqi W, Jianying M et al (2010) Automatic segmentation of calcifications in intra-vascular ultrasound images using snakes and the contourlet transform. Ultrasound Med Biol 36(1):111–129